npj | Quantum Information

www.nature.com/npjqi

ARTICLE OPEN

Connecting Fano interference and the Jaynes-Cummings model in cavity magnonics

Jakob Gollwitzer[1], Lars Bocklage[1,2✉], Ralf Röhlsberger[1,2,3,4,5] and Guido Meier[2,6]

We show that Fano interference can be realized in a macroscopic microwave cavity coupled to a spin ensemble at room temperature. Via a formalism developed from the linearized Jaynes-Cummings model of cavity electromagnonics, we show that generalized Fano interference emerges from the photon–magnon interaction at low cooperativity. In this regime, the reflectivity approximates the scattering cross-section derived from the Fano-Anderson model. Although asymmetric lineshapes in this system are often associated with the Fano formalism, we show that whilst Fano interference is actually present, an exact Fano form cannot be achieved from the linear Jaynes-Cummings model. In the Fano model an additional contribution arises, which is attributed to decoherence in other systems, and in this case is due to the resonant nature of the photonic mode. The formalism is experimentally verified and accounts for the asymmetric lineshapes arising from the interaction between magnon and photon channels. As the magnon–photon coupling strength is increased, these channels merge into hybridized magnon–photon modes and the generalized Fano interference picture breaks down. Our results are universally applicable to systems underlying the linearized Jaynes-Cummings Hamiltonian at low cooperativity and connect the microscopic parameters of the quantum optical model to generalized Fano lineshapes.

npj Quantum Information (2021)7:114 ; https://doi.org/10.1038/s41534-021-00445-8

INTRODUCTION

Resonances in atoms, molecules, or matter reflect many of their properties. Coupling of resonances to the environment or to other resonances leads to emerging phenomena in a large variety of systems. Spurred by the possibility of coherent photon–magnon interaction and associated potential for quantum information processing, the field of cavity electromagnonics has experienced enormous growth in the past decade[1]. A single photonic mode can be strongly coupled to a single magnon mode[2,3]. Classical coherence effects reproduce the behavior predicted by quantum optical models both at cryogenic and at room temperatures[3,4]. Strong magnon–photon coupling via the so-called cavity-magnon polariton has been vital to reaching photon detection via electrical spin pumping probes[5], dark mode memories[6], and magnon coupling to a qubit[7]. Invoking the description of the polariton as a classical interaction between an electromagnetic wave and a matter polarization[8], strong magnon–photon coupling may be understood as the hybridization of the magnonic and photonic modes[9].

For classically coupled harmonic oscillators, interesting behavior of the coupled resonances also emerges when the damping dominates over the coupling strength. For such classical systems, it has been shown that Fano interference occurs[10,11] at and around the exceptional point[12]. Based on the quantum picture of magnon–photon interaction, magnetically induced transparency (MIT) and the Purcell effect have been demonstrated[3]. These effects may be described as interference phenomena associated with the Fano effect[13]. Experiments on magnon–photon interactions show the existence of asymmetric lineshapes, which are associated with Fano resonances[9,13–15]. Our study connects the quantum model of cavity electromagnonics based on the linearized Jaynes-Cummings (JC) Hamiltonian to the Fano interference picture. The model links the cavity electromagnonics and the Fano models in a physically meaningful way. It also shows that a standard Fano model cannot account for either the cavity resonance or the magnon–photon coupling. We introduce a generalized Fano model that adequately describes the asymmetric lineshapes and reveals the physics that connects the linearized JC model to Fano interference at low coupling strength.

Fano resonances emerge when a discrete state falls within the band of continuum states. The fingerprint of the Fano effect is a characteristic asymmetric lineshape. Coupling between the resonant and continuum states is described by the configuration interaction, which mixes the discrete and continuum states of the system[16]. The Fano effect involves interference between these mixed states and a discrete resonant state. Well-defined phases of a background channel and a resonant channel are required to unambiguously identify the Fano effect. The Fano-Anderson Hamiltonian[17]

$$\mathcal{H} = \hbar\omega_b b^\dagger b + \hbar\sum_k \omega_{c,k} c_k^\dagger c_k + \sum_k A_k\left(b^\dagger c_k + c_k^\dagger b\right) \quad (1)$$

is used to describe the interaction of a discrete magnon state with a photonic continuum[15]. Here, b and c are the bosonic operators of the discrete and continuum states, respectively. The mode coupling strength is given by A_k. The scattering cross-section of the Fano resonance is[16]

$$\sigma = \sigma_0 \frac{(\varepsilon + q)^2}{\varepsilon^2 + 1} \quad (2)$$

where $\varepsilon = (E - E_0)/\gamma$ is the dimensionless resonant channel detuning with resonance energy E_0, q is the asymmetry parameter, $\gamma = \Gamma/2$ is the linewidth of the Fano resonance with damping parameter Γ, and σ_0 is the resonant cross-section. In the

[1]Deutsches Elektronen-Synchrotron DESY, Hamburg, Germany. [2]The Hamburg Centre for Ultrafast Imaging, Hamburg, Germany. [3]Institut für Optik and Quantenelektronik, Friedrich-Schiller-Universität Jena, Jena, Germany. [4]Helmholtz Institut Jena, Jena, Germany. [5]Helmholtz Centre for Heavy Ion Research (GSI), Darmstadt, Germany. [6]Max-Planck Institute for the Structure and Dynamics of Matter, Hamburg, Germany. ✉email: lars.bocklage@desy.de

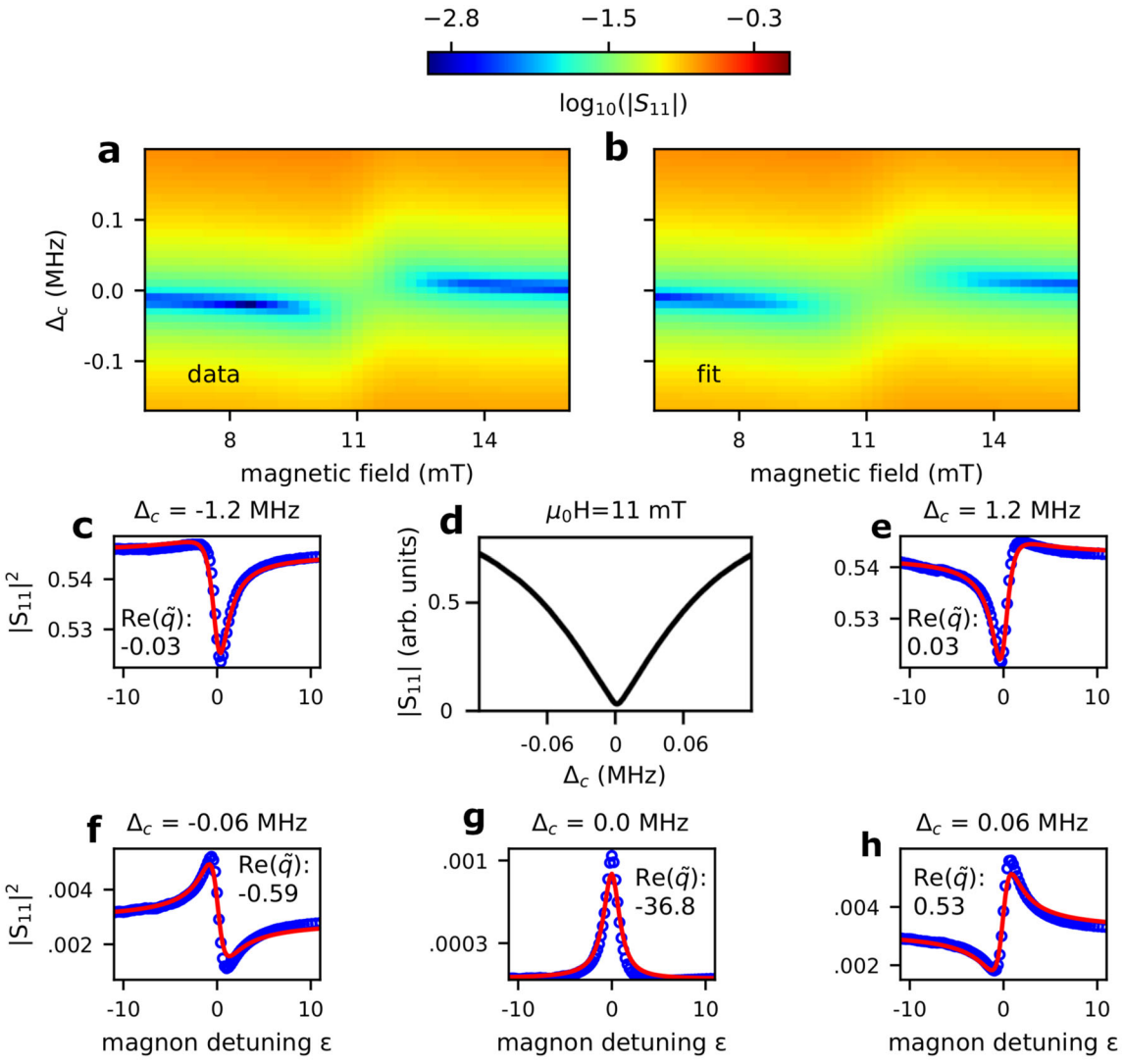

Fig. 1 Cavity reflectivity of the interaction between the microwave cavity mode and the magnon mode. a Magnitude of the measured reflectivity showing the Purcell effect for a thin 10 nm thick permalloy film inserted into the cavity. The Kittel mode of the permalloy film couples to the cavity photon, which is manifested as a distortion in the cavity resonance. A fit of the reflectivity via Eq. (5) is shown in (**b**). The physical quantities extracted from the fit and fits of the reflectivity performed for permalloy thicknesses of 40 nm and 200 nm are given in the Supplementary Table 1. **d** The fixed field lineshape at the resonant field of the Kittel mode. Fixed frequency lineshapes as a function of the dimensionless magnon detuning for various cavity detunings are shown as open blue circles in (**c**, **e**–**h**). The fits of the lineshapes are performed in accordance with Eq. (6) as discussed in the text and are featured as red lines. The corresponding $\mathrm{Re}(\tilde{q})$ value is shown next to each fit.

standard Fano form q is real. In case of a complex $\tilde{q}$, as required in the present case, the imaginary part signifies a contribution to the scattering cross-section typically associated with dephasing or dissipation[18,19] such that

$$\sigma = \sigma_0 \frac{|\varepsilon + \tilde{q}|^2}{\varepsilon^2 + 1} = \sigma_0 \left(\frac{(\varepsilon + \mathrm{Re}(\tilde{q}))^2}{\varepsilon^2 + 1} + \frac{\mathrm{Im}(\tilde{q})^2}{\varepsilon^2 + 1} \right) \tag{3}$$

In contrast to the magnon resonance coupled to a photonic continuum in the Fano-Anderson model stands the strong coupling of two-level system and a harmonic resonance as described by the JC model[3]. With appropriate modifications, this JC model is employed to describe magnon–photon coupling in cavity electromagnonics. Specifically, at high polarization as is present in a homogeneously magnetized ferromagnetic element, a collection of two-level systems and a collection of harmonic oscillators behave identically. This is described by the linearized Holstein-Primakoff transformation[20], which treats magnonic excitations as non-interacting bosonic quasiparticles. The so-called linearized JC Hamiltonian underlying the linearized Holstein Primakoff transformation is written as

$$\mathcal{H} = \hbar\omega_b b^\dagger b + \hbar\omega_c c^\dagger c + \mathrm{i}\hbar g\left(b^\dagger c + c^\dagger b\right) \tag{4}$$

which is a common starting point in the field of cavity electromagnonics and also applies to the system studied in this work. Here, g is the coupling strength in terms of frequency. The two resonances can reversibly interchange energy in the case of strong coupling, which leads to an avoided crossing of the modes and Rabi oscillations. However, when damping dominates, the magnon–photon interaction becomes irreversible. A striking difference between the linearized JC model and the Fano-Anderson model is that in the latter the resonance lies within a continuum of states and energy exchange is intrinsically irreversible[21]. Similarity of the two models should therefore be expected when the coupling strength g of the linearized JC model

is low and the magnon–photon system does not periodically exchange energy.

In this work, we show that Fano interference emerges in the lineshapes of the reflectivity of a coupled magnon–photon system described by the linearized JC Hamiltonian at low coupling strength. We measure the evolution of Fano interference in a coupled magnon–photon system usually used to investigate the cavity-magnon polariton. In addition, we describe the transition of the system from the Fano description of interference between channels to hybridization of modes as the cooperativity is increased. The resonant nature of the cavity generates an imaginary part of the asymmetry parameter $\tilde{q}$. The Fano description of interfering channels only becomes visible within the generalized Fano model developed here. Although the model highly resembles the typical Fano scattering formalism, we show that only the generalized Fano model accounts for the magnon–photon interactions in the JC model at low cooperativity.

The reflectivity from a microwave cavity in which the interaction between a photon and a magnon is described by the linearized JC Hamiltonian can be expressed in terms of the cavity detuning $\Delta_c = \omega_c - \omega$, the magnon detuning $\Delta_m = \omega_m - \omega$, the magnon damping rate γ, the cavity damping rate κ, and the coupling strength g. The energy-dependent reflectivity at critical coupling according to the linearized JC Hamiltonian is[3]

$$r(\Delta_c, \Delta_m) = -1 + \frac{\kappa}{\mathrm{i}\Delta_c + \kappa + \frac{g^2}{\mathrm{i}\Delta_m + \gamma}} \tag{5}$$

which has been obtained via the Heisenberg-Langevin approach using the input–output formalism. The latter describes the interaction between a cavity system and its environment by allowing the system to couple to a continuum of environmental modes. The reflectivity in Eq. (5) arises in all cavity-based systems underlying the linearized JC model and hence occurs in a multitude of systems. For instance, this behavior is found in quantum dots coupled to a cavity[22], a condensate of ^{87}Rb atoms coupled to an optical cavity[23], an ensemble of nitrogen vacancy centers in diamond interacting with a superconducting resonator[24], as well as Mössbauer nuclei embedded in a cavity for X-rays[25,26]. In this work, an explicit connection between Eq. (5) and a generalized form of Fano interference will be presented.

RESULTS

Generalized Fano form

The absolute value of the reflectivity $|r(\Delta_m, \Delta_c)|$ of a $t = 10$ nm thick permalloy ($Ni_{80}Fe_{20}$) film inserted into the cavity is shown in Fig. 1a. The linewidth of magnetic damping of permalloy used in this study is $\gamma \approx 200$ MHz and thus much larger than the linewidth of the cavity $\kappa \approx 1$ MHz. The coupling strength g is determined by the amount of magnetic material and spin density[3] of permalloy and is of the order of several MHz so that the experiment is performed in the Purcell regime where $\gamma > g > \kappa$. Thus, the cooperativity $C = g^2/\kappa\gamma$ is always below one.

Fig. 1b shows the fit of the reflectivity via Eq. (5). The fit parameters include γ, κ, and g and are listed in the Supplementary Table 1. The best-fit values confirm that cavity photon–magnon interactions occur in the Purcell regime and that the coupling strength g is proportional to the square root of the permalloy thin-film thickness as expected. Field swept lineshapes for fixed cavity detuning are shown for a few cavity detunings in Fig. 1c, e–h. On cavity resonance ($\Delta_c = 0$, Fig. 1g), the lineshape is a symmetric peak. Measurements are conducted for a magnonic detuning range Δ_m determined by an external magnetic field, which sets the ferromagnetic resonance frequency ω_m governed by the Kittel formula for an extended soft ferromagnetic thin film. When the cavity is detuned, the lineshape acquires an asymmetric shape that resembles Fano interference.

Although Eq. (5) describes the reflectivity well, it gives neither insight into whether the fixed frequency lineshapes are due to Fano interference nor if a connection between the linearized JC model and the Fano model exist. To obtain this insight, the squared amplitude of the reflectivity of Eq. (5) is transformed to a generalized Fano form (see Supplementary Methods)

$$|r(\varepsilon)|^2 = \sigma_0 \left(\frac{(\varepsilon + \mathrm{Re}(\tilde{q}))^2}{\varepsilon^2 + \eta^2} + \frac{\mathrm{Im}(\tilde{q})^2}{\varepsilon^2 + \eta^2} \right), \tag{6}$$

which describes the fixed frequency lineshapes as a function of dimensionless magnon detuning $\varepsilon = -\Delta_m/\gamma$ in all coupling regimes. The resonant scattering cross-section $\sigma_0 = (1 + \kappa^2/\Delta_c^2)^{-1}$ gives the inverse Lorentzian resonant reflection of the cavity, on which the spectral signature of the magnon–photon interaction is imprinted. Here, the complex asymmetry parameter $\tilde{q} = C\kappa/\Delta_c + \mathrm{i}$ determines the asymmetry of the fixed frequency lineshapes via $\mathrm{Re}(\tilde{q})$, which depends inversely on cavity detuning. The imaginary part of the asymmetry parameter is $\mathrm{Im}(\tilde{q}) = 1$ and hence does not exhibit a functional dependence on external parameters. The parameter $\eta = \sqrt{1 + f(\varepsilon, \Delta_c, C)}$ depends on the cavity and magnon detuning as well as on the cooperativity. For details of the calculation explicitly connecting the reflectivity to the generalized Fano form see the Supplementary Methods. The additional term η approaches $\eta^2 \approx 1$ for decreasing coupling strength but generally introduces a difference to the standard Fano model. It describes the coupling of magnon and photon modes. Because Eq. (6) is a reformulation of the reflectivity given in Eq. (5), this formula is valid at all coupling regimes.

The experimentally observed fixed frequency lineshapes presented in Fig. 1 are fit using Eq. (6), showing excellent agreement. Inverse dependence of $\mathrm{Re}(\tilde{q})$ on cavity detuning Δ_c is shown in Fig. 2 resulting from the fits of $\mathrm{Re}(\tilde{q})$ to the lineshapes (blue circles). The exact same dependence is observed with the cooperativity and damping obtained from fits of the reflectivity via Eq. (5) (red line, see Supplementary Methods). We note that such an inverse dependence of the asymmetry parameter on the cavity detuning in the cavity reflectivity is also evident in Fano lineshapes between hard X-ray cavities and the Mössbauer resonance of ^{57}Fe[26]. The linear dependence of $\mathrm{Re}(\tilde{q})$ on the cooperativity C is visible in Fig. 2d.

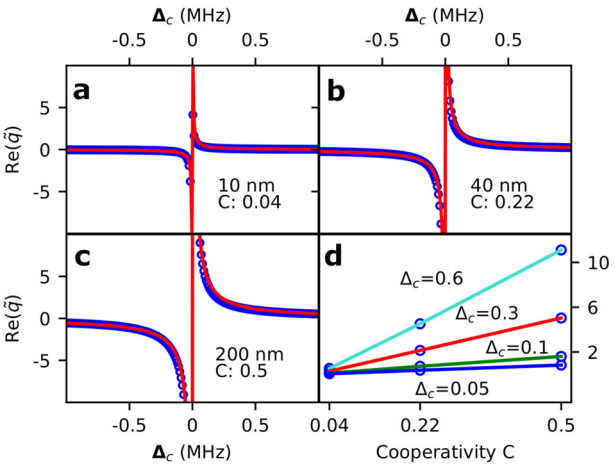

Fig. 2 Behavior of the real part of the asymmetry parameter $\mathrm{Re}(\tilde{q})$. a–c The dependence of $\mathrm{Re}(\tilde{q})$ on cavity detuning Δ_c for the case of 10, 40, and 200 nm thick permalloy film. The blue circles are $\mathrm{Re}(\tilde{q})$ values obtained via a fit of the fixed frequency lineshapes using Eq. (6). The red curves represent the behavior of $\mathrm{Re}(\tilde{q}) = C\kappa/\Delta_c$ based on the generalized Fano model discussed in the text. **d** The linear dependence of $\mathrm{Re}(\tilde{q})$ on the cooperativity at the various cavity detunings indicated and given in MHz.

Equation (6) exhibits a strong similarity to the description of Fano interference in the presence of decoherence, namely Eq. (3) with a complex $\tilde{q}$. For increased cooperativity or magnon detuning, the deviation from Fano lineshapes becomes more pronounced. At low cooperativity, however, $\eta^2 \approx 1$ and the standard complex Fano relation (3) is recovered. Then, the first term in the parentheses represents the coherent part of the standard Fano form. The second term connected to the imaginary part of $\tilde{q}$ is a Lorentzian that peaks on magnon resonance. As $\mathrm{Im}(\tilde{q})$ is a constant, the relative coherent contribution to the fixed frequency lineshapes is set by $\mathrm{Re}(\tilde{q})$. The ratio of both contributions to the generalized Fano lineshape is given by $\mathrm{Re}(\tilde{q})/\mathrm{Im}(\tilde{q}) = g^2/\gamma\Delta_c$, which denotes that as cavity detuning Δ_c increases, the relative contribution of $\mathrm{Im}(\tilde{q})$ to the spectral signature increases. The constant form of $\mathrm{Im}(\tilde{q})$ stands in contrast to other studies of generalized Fano interference in which phase shifts, dephasing, or dissipation are introduced that change both the real and imaginary parts of $\tilde{q}$[18,27,28]. The coupling between a single magnon and a single photon mode makes the magnon–photon system fundamentally different to the Fano interference encountered when a matter resonance lies within a continuum of states. The JC model is coherent, with dissipation handled via input–output formalism and the intrinsic damping constants of the modes. Thus, we do not expect additional decoherence, explaining the constant form of $\mathrm{Im}(\tilde{q})$.

The contribution of $\mathrm{Im}(\tilde{q})$ to the generalized Fano lineshapes is attributed to the resonant nature of the photonic mode. The resonance of the cavity signifies that photons are increasingly reflected by the cavity as it is detuned. This is described via the scattering cross-section σ_0, which represents the spectral response of the empty microwave cavity. Hence, σ_0 describes the probability of a photon entering the cavity as a function of cavity detuning Δ_c, with fewer and fewer photons able to enter the cavity as Δ_c increases. However, the behavior of σ_0 does not explain the detuning-dependent size of the spectral feature in the fixed-frequency lineshapes. For large detuning of the cavity, all incoming photons are reflected and a flat line without any spectral feature evolves. In the limit of large cavity detuning, the reflectivity is $|r(\varepsilon)|^2 \approx (\varepsilon^2+1)/(\varepsilon^2+\eta^2)$, which approaches unity for $\eta^2 \approx 1$, and the spectral features vanish. A functional dependence of real and imaginary parts of $\tilde{q}$ on each other, as in cases of incoherent processes[27], is not present here. In the present case, the imaginary part is essential to obtain the correct reflectivity of the cavity and spectral features but is not related to decoherence. It rather is the addition of the resonant photonic mode behavior to the Fano model that normally describes a photonic continuum. The factor n emerges from magnon–photon coupling, which also stands in contrast to the Fano picture of interfering and non-coupled channels. The mode coupling is actually responsible for the dip-like spectral feature at large cavity detuning, which cannot be explained by the vanishing real part if the imaginary part is unity[18].

Fano interference

Central to the Fano lineshape is its interpretation as an interference phenomenon between two scattering channels with well-defined phases. The magnon–photon coupling regimes for which the lineshape may be interpreted as Fano interference is determined by the cooperativity and the detunings via $\eta(\varepsilon, \Delta_c, C)$. Under the assumption that η is real, the fixed frequency lineshapes can be written in an interference picture by reformulating Eq. (6)

$$|r(\varepsilon)|^2 = \sigma_0\left(\left|e^{i\varphi_c} + \frac{|\mathrm{Re}(\tilde{q}) - i\eta|}{\sqrt{\varepsilon^2+\eta^2}}e^{i\varphi_m}\right|^2 + \frac{\mathrm{Im}(\tilde{q})^2}{\varepsilon^2+\eta^2}\right) \quad (7)$$

where $\varphi_c = -\arg(\mathrm{Re}(\tilde{q}) - i\eta)$and $\varphi_m = \arg(\varepsilon - i\eta)$ are the cavity and magnon channel phases, respectively. The asymmetry parameter is thus mapped to a universal phase factor[29]. This equation is valid in the Purcell and MIT regime. The first term in the parentheses describes Fano interference, whereas the last term adds the resonance of the cavity to the Fano model. In the spirit of previous works on Fano resonance[26], we interpret the two terms in absolute value bars as interference between a photonic background channel set by the cavity and the discrete magnon resonance coupled to the cavity. This separation is possible because at low coupling strength the modes can be treated as almost independent. Radiation is input into the cavity at a fixed cavity detuning value Δ_c while the magnon channel phase φ_m progresses form $-\pi$ to 0 as the magnonic detuning is swept through the magnon resonance. The interference between these channels results in characteristic Fano resonances with the asymmetry defined by the background phase φ_c, which is set by the cavity detuning. The phase of the cavity background channel is set by its detuning and thus the asymmetry can be controlled. The situation differs when the transmission spectrum is calculated. In this case, one obtains a similar spectrum as Eq. (6) but with the scattering cross-section for transmission $\sigma_0^t = (1+\Delta_c^2/\kappa^2)^{-1}$ and with a constant asymmetry parameter $\mathrm{Re}(\tilde{q}) = 0$. For transmission, the cavity phase is always $\pi/2$ despite the cavity detuning. The difference between transmission and reflection channel can be understood in terms of their interference with magnon resonance in the cavity (see Supplementary Methods).

For the 10 nm film, the cavity phase φ_c determined from the fits shown in Fig. 1 is plotted in Fig. 3d, e as a function of $\mathrm{Re}(\tilde{q})$ and Δ_c. Of the measured samples, only for the 10 nm film the cooperativity is small enough so that no variation in φ_c occurs in the investigated detuning range. In the Fano model, the background phase sets the form of the spectrum and yields asymmetric fixed frequency lineshapes when φ_c is not a multiple of $\pi/2$. In the model, φ_c is independent of resonant channel detuning.

Despite deviations from the standard Fano formalism with a purely real $\tilde{q}$ that are caused by the imaginary part due to the cavity, Fano interference between the magnon and photon channels emerges at low cooperativity. At zero cavity detuning, photon input into the cavity is maximal and the standard Fano term alone determines the fixed frequency lineshapes. In this limit, the photonic mode mimics a broad continuum of modes without any influence of the imaginary part as $\mathrm{Re}(\tilde{q}) \to \infty$, because no photons are reflected and all incoming photons probe the magnon–photon interaction. The lineshape reduces to a Lorentzian as predicted by Eq. (2), which is indicative of the Purcell broadening of the cavity resonance. Rapid changes in the cavity phase in the region $|\Delta_c| \lesssim \kappa C$ yields a rapid transformation from a Lorentzian to an asymmetric lineshape. These lineshapes exhibit a large contribution from $\mathrm{Re}(\tilde{q})$ with values decreasing to unity. The increased reflection of photons from the cavity modifies the spectral features due to the cavity resonance via $\mathrm{Im}(\tilde{q})$. The cavity phase is fixed for each lineshape. In the limit of very large cavity detuning, $|\Delta_c| \to \infty$, all photons are reflected, and no spectral signatures arise (not shown). At intermediate cavity detunings $|\Delta_c| \gtrsim \kappa C$ (shown at $\Delta_c = \pm$ 1.2 MHz in Fig. 1), almost symmetric dips occur with their amplitude depending on the mode coupling term η. These dips are understood in terms of the Purcell effect where the photonic dissipation is altered while the magnon is swept over its resonance.

When the cooperativity is increased, as for the 40 and 200 nm films, η becomes purely imaginary for certain magnon and cavity detunings. In Fig. 3a–c, the cavity phase φ_c calculated from the parameters obtained from the fit plotted in Fig. 1 are shown for permalloy films with thicknesses of 10, 40, and 200 nm. For the 10 nm thick film, φ_c is effectively constant over the investigated magnon detuning range so that the Fano interpretation of Eq. (7) is valid. In contrast, for the 200 nm thick film φ_c is no longer independent of magnon detuning. Rather, the cavity phase depends on magnon detuning via the mode coupling term η. Here, photon–magnon hybridization starts to manifest so that the physical interpretation of Fano interference of two weakly coupled

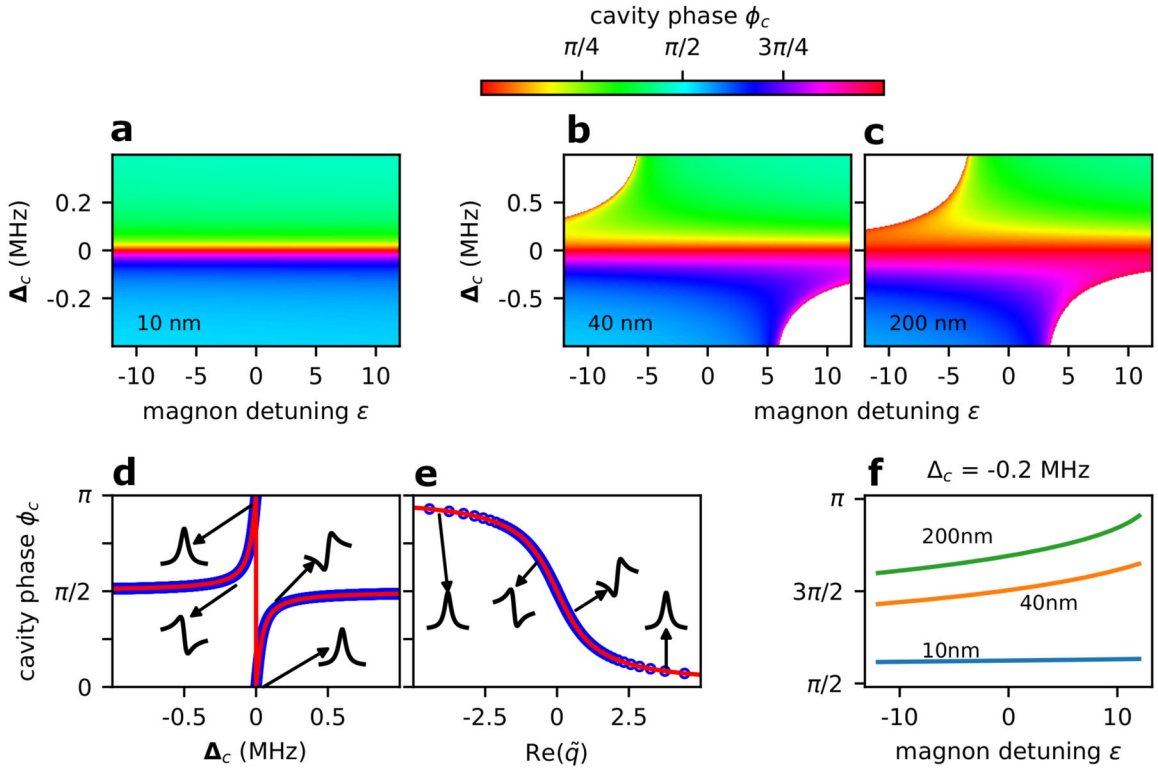

Fig. 3 The Fano interference picture. The cavity background channel phase φ_c as calculated from Eq. (7) with the experimentally determined parameters is shown in dependence on the cavity and magnon detunings for the case of (**a**) 10 nm, (**b**) 40 nm, and (**c**) 200 nm thick permalloy film inserted into the cavity. The white regions in (**b**) and (**c**) correspond to regions in which η becomes imaginary. **d**, **e** The cavity phase for the 10 nm film at zero dimensionless magnon detuning as a function of cavity detuning and Re($\tilde{q}$), respectively. The blue open dots represent the cavity phase calculated on the basis of fits of the fixed frequency lineshapes, whereas the red lines represent the cavity phase of the theoretical Fano interference picture with $\eta = 1$. **f** The cavity phase at cavity detuning $\Delta_c = -0.2$ MHz for the three thicknesses investigated. Note that only for the case $t = 10$ nm the cavity phase is essentially constant as a function of magnon detuning.

and interfering channels is no longer accurate. Fano interference can be recovered at low cooperativity only.

DISCUSSION

The results presented here show that at low cooperativity, the linearized Jaynes-Cummings (JC) model leads to lineshapes that strongly resemble those characteristic of Fano interference. The similarity of the Fano scattering cross-section as derived from the Fano-Anderson Hamiltonian and the linearized JC Hamiltonian at low coupling strength is evident. A common thread between these models is the scattering of the incoming photon via a mixed state containing both discrete-state and continuum-state contributions. However, while the linearized JC model describes scattering into a single photonic mode, the Fano-Anderson model describes scattering into a continuum of photonic modes. At low cooperativity, the magnon–photon coupling from the linearized JC Hamiltonian is barely reversible and thus almost coincides with the irreversible scattering into a continuum in the Fano-Anderson model. The main difference is the contribution that arises from the resonant nature of the photonic cavity mode and stands in contrast to the dispersionless continuum. At higher cooperativities the magnon–photon modes hybridize, eventually merging into the strong coupling regime, and the Fano interpretation breaks down.

Asymmetric lineshapes are not necessarily connected to Fano interference even though the equations resemble the Fano form (see Eq. (5)). Only the interference picture of Eq. (7) gives insight into whether the underlying physics are based on Fano interference. Especially in the context of two coupled resonances, the resonant photonic mode of the cavity and the mode coupling have to be accounted for properly. Control of the Fano parameters is given by the cavities' detuning dependence of the scattering cross-section σ_0 and the background channel phase φ_c.

In conclusion, we show that a generalized Fano form emerges from the linearized JC model and verify this experimentally in a microwave cavity coupled to the Kittel mode of a permalloy film in the Purcell regime. Our model connects the microscopic parameters of the linearized JC model to the phenomenological parameters of the generalized Fano form and uncovers magnon–photon coupling at low cooperativity as interference between scattering of a background cavity channel and the magnon channel. These two channels have well-defined phases in accordance with the Fano interference picture. This is remarkable as it shows that the physics of Fano interference surfaces even though the system consists of two coupled modes with finite linewidths. We thus open a new perspective in the connection between the Fano-Anderson and the linearized JC models at low cooperativities. Depending on the coupling strength, the magnon–photon coupling can be understood in terms of either Fano interference or mode hybridization. Finally, the linear JC model describes many types of systems in which a cavity mode interacts weakly with a matter-based harmonic resonance. The wide applicability of the linear JC model hence makes the results presented here important to many areas of physics including hard X-ray quantum optics, atomic interactions with optical cavities, and cavity electromagnonics.

METHODS

Experimental setup

To experimentally obtain Fano profiles, we perform reflectivity measurements of a microwave cavity in which microwave photons are coupled to magnons in a metallic, ferromagnetic thin film. We measure the complex

reflectivity of the microwave cavity using a vector network analyzer (S_{11} parameter) on a permalloy thin film placed in a rectangular microwave cavity operated in the TE101 mode at $\omega_{res}/2\pi \approx 3090$ MHz. A static magnetic field H_{ext} biases the permalloy thin film to set the magnonic resonance frequency in accordance with the Kittel relation for a magnetic thin film[30]. Measurements are performed for a cavity detuning of $\Delta_c = \pm 10$ MHz around the cavity resonance frequency of 3090 MHz and for a magnonic detuning range Δ_m determined by the external magnetic field, which sets the ferromagnetic resonance frequency. The microwave cavity is machined out of oxygen-free copper and has a linewidth $\kappa/2\pi$ (HWHM) of 1.13 MHz so that the cavity has a Q-factor of ≈2700 at room temperature. Power is input into the cavity via a terminal stub, the length of which has been adjusted to ensure critical coupling. The complex reflectivity of the cavity is obtained for permalloy films of 10, 40, and 200 nm thickness placed in the cavity. The absolute value of the reflectivity on the detuning grid is shown in the Supplementary Fig. 2, where a fit performed using Eq. (5) together with the fit parameters and further details of the experiment are shown.

DATA AVAILABILITY

The data that support the findings of this study are available from the corresponding author upon reasonable request.

Received: 3 February 2021; Accepted: 9 June 2021;
Published online: 19 July 2021

REFERENCES

1. LaChance-Quirion, D., Tabuchi, Y., Gloppe, A., Usami, K. & Nakamura, Y. Hybrid quantum systems based on magnonics. *Appl. Phys. Express* **12**, 070101 (2019).
2. Soykal, Ö. O. & Flatté, M. E. Strong field interactions between a nanomagnet and a photonic cavity. *Phys. Rev. Lett.* **104**, 077202 (2010).
3. Zhang, X., Zou, C.-L., Jiang, L. & Tang, H. X. Strongly coupled magnons and cavity microwave photons. *Phys. Rev. Lett.* **113**, 156401 (2014).
4. Zhang, D. et al. Cavity quantum electrodynamics with ferromagnetic magnons in a small yttrium-iron-garnet sphere. *npj Quantum Inf.* **1**, 15014 (2015).
5. Bai, L. et al. Spin pumping in electrodynamically coupled magnon photon systems. *Phys. Rev. Lett.* **114**, 227201 (2015).
6. Zhang, X. et al. Magnon dark modes and gradient memory. *Nat. Commun.* **6**, 8914 (2015).
7. Kubo, Y. et al. Strong coupling of a spin ensemble to a superconducting resonator. *Phys. Rev. Lett.* **105**, 140502 (2010).
8. Huang, K. On the interaction between the radiation field and ionic crystals. *Proc. Math. Phys. Eng. Sci.* **208**, 352–365 (1951).
9. Harder, M. & Hu, C.-M. Cavity spintronics: an early review of recent progress in the study of magnon–photon level repulsion. *Solid State Phys.* **69**, 47–121 (2018).
10. Joe, Y. S., Satanin, A. M. & Kim, C. S. Classical analogy of Fano resonances. *Phys. Scr.* **74**, 2 (2006).
11. Schwarz, L., Cartarius, H., Wunner, G., Heiss, W. D. & Main, J. Fano resonances in scattering: an alternative perspective. *Eur. Phys. J. D* **69**, 196 (2015).
12. Harder, M., Bai, L., Hyde, P. & Hu, C.-M. Topological properties of a coupled spin-photon system induced by damping. *Phys. Rev. B* **95**, 214411 (2017).
13. Limonov, M., Rybin, M. V., Poddubny, A. N. & Kivshar, Y. S. Fano resonances in photonics. *Nat. Photonics* **11**, 543–554 (2017).
14. Kamenetskii, E. O., Vaisman, G. & Shavit, R. Fano resonances of microwave structures with embedded magneto-dipolar quantum dots. *J. Appl. Phys.* **114**, 173902 (2013).
15. Yao, B. et al. Coherent control of magnon radiative damping with local photon states. *Commun. Phys.* **2**, 161 (2019).
16. Fano, U. Effects of configuration interaction on intensities and phase shifts. *Phys. Rev.* **124**, 1866–1878 (1961).
17. Mahan, G. D. *Many Particle Physics* 3rd edn (Plenum Press, 2000)
18. Finkelstein-Shapiro, D. et al. Fano-Liouville spectral signatures in open quantum systems. *Phys. Rev. Lett.* **115**, 113006 (2015).
19. Clerk, A., Waintal, X. & Brouwer, P. W. Fano resonances as a probe of phase coherence in quantum dots. *Phys. Rev. Lett.* **86**, 4636–4639 (2001).
20. Kurucz, Z., Wesenberg, J. H. & Mølmer, K. Spectroscopic properties of inhomogeneously broadened spin ensembles in a cavity. *Phys. Rev. A* **83**, 053852 (2011).
21. Nicolaides, C. A. Irreversibility in the framework of Hermitian and non-Hermitian treatments of resonance states. In *Irreversible Quantum Dynamics. Lecture Notes in Physics* Vol. 622 (eds Benatti, F. & Floreanini, R.) 357–369 (Springer, 2003)
22. Englund, D. et al. Controlling cavity reflectivity with a single quantum dot. *Nature* **450**, 857–861 (2007).
23. Brennecke, F. et al. Cavity QED with a Bose-Einstein condensate. *Nature* **450**, 268–271 (2007).
24. Kubo, Y. et al. Strong coupling of a spin ensemble to a superconducting resonator. *Phys. Rev. Lett.* **105**, 140502 (2010).
25. Röhlsberger, R., Wille, H.-C., Schlage, K. & Sahoo, B. Electromagnetically induced transparency with resonant nuclei in a cavity. *Nature* **482**, 199–203 (2012).
26. Heeg, K. P. et al. Interferometric phase detection at X-ray energies via Fano resonance control. *Phys. Rev. Lett.* **114**, 207401 (2015).
27. Bärnthaler, A. et al. Probing decoherence through Fano resonances. *Phys. Rev. Lett.* **105**, 056801 (2010).
28. Kobayashi, K., Aikawa, H., Katsumoto, S. & Iye, Y. Mesoscopic Fano effect in a quantum dot embedded in an Aharonov-Bohm ring. *Phys. Rev. B* **68**, 235304 (2003).
29. Ott, C. et al. Lorentz meets Fano in spectral line shapes: a universal phase and its laser control. *Science* **340**, 716–720 (2013).
30. Nahrwold, G. et al. Structural, magnetic, and transport properties of permalloy for spintronic experiments. *J. Appl. Phys.* **108**, 013907 (2010).

ACKNOWLEDGEMENTS

We thank Andrey Siemens and Michael Volkmann for excellent technical support. We acknowledge the support of the Helmholtz Association through project-oriented funds. This work is supported by the Cluster of Excellence "The Hamburg Centre for Ultrafast Imaging" of the Deutsche Forschungsgemeinschaft (DFG) - EXC 1074 - project ID 194651731. Financial support of the Graduiertenforderungsprogramm der Universität Hamburg is gratefully acknowledged. All figures and pictures by the authors under a CC BY 4.0 license.

AUTHOR CONTRIBUTIONS

J.G. and L.B. conceived and performed the experiment, developed the theoretical model and performed analytical calculations. J.G. prepared the samples and analyzed the data. G.M. and R.R. supervised the project. J.G. wrote the manuscript with contributions from all authors.

FUNDING

Open Access funding enabled and organized by Projekt DEAL.

COMPETING INTERESTS

The authors declare no competing interests.

ADDITIONAL INFORMATION

Supplementary information The online version contains supplementary material available at https://doi.org/10.1038/s41534-021-00445-8.

Correspondence and requests for materials should be addressed to L.B.

Reprints and permission information is available at http://www.nature.com/reprints

Publisher's note Springer Nature remains neutral with regard to jurisdictional claims in published maps and institutional affiliations.